

# Site characterization using surface wave methods in the Arsin-Trabzon province, NE Turkey

Özgeç Akin<sup>1</sup> · Nilgün Sayil<sup>1</sup>

Received: 6 June 2014 / Accepted: 17 July 2015 / Published online: 21 December 2015  
© Springer-Verlag Berlin Heidelberg 2015

**Abstract** Trabzon-Arsin located in the eastern Black Sea region is situated approximately 150 km away from North Anatolian Fault zone and under the effect of the overthrust zone along the shoreline, and the faults located onshore. In the study area where the new residential areas are planned to be established by filling the sea, it is required to know soil conditions accurately and in detail. In this study, the soil predominant period ( $T_M$ ) and  $H/V$  spectral ratio obtained by Nakamura method have been found between 0.1 and 0.37 s and 1–8, respectively. The soil predominant period ( $T_R$ ),  $V_S$  and bedrock depth obtained by MASW method are between 0.1 and 0.36 s, 162–1376 m/s and 10–15 m, respectively. According to determined  $V_S$  values,  $V_{S30}$  and  $V_{S10}$  values calculated. Thus, the study area classified by the help of  $V_{S30}$  and characterized for base depth (10 m) of buildings more accurately. The average amplification values of 1.56, 2.10 and 1.30 have been found for three empirical relationships.

**Keywords** Microtremor · Nakamura ( $H/V$ ) spectral ratio method · MASW method · Soil parameters · Arsin-Trabzon

## Introduction

Almost all of the shearing strengths such as elasticity module, incompressibility module, natural vibration frequency, seismic amplification coefficient, Poisson's ratio

and even more soil dynamic parameters are related directly to shear-wave velocity ( $V_S$ ).  $V_S$  values are used in determining the dynamic soil behavior, especially together with soil predominant period and soil amplification. One of the most preferred methods for determining  $V_S$  values is multi-channel analysis of surface waves (MASW) method (Joyner and Furnal 1984; Borchardt et al. 1991; Bonilla et al. 1997; Park et al. 1999; Liu et al. 2000; Louie 2001; Okada 2003). The general principle in surface wave methods is the utilization of dispersive characteristic of surface waves recorded by passive (environmental noise) or active (horizontal or vertical) sources. MASW method that is one of the most effective active-source surface wave methods is used to determine the soil characterization up to 30 m.

Another method used for obtaining the predominant period (or frequency) of soil is single-station Nakamura  $H/V$  spectral method (Nakamura 1989). This method is widely used, especially for determining the predominant period of the soil for the purpose of seismic microzonation (e.g., Nogoshi and Igarashi 1971; Bour et al. 1989; Parolai et al. 2001; Pando et al. 2008; Rodriguez and Midorikawa 2002; Rastogi et al. 2011; Leyton et al. 2013; Singh et al. 2014). In recent years, this method became the preferred method for obtaining resonance frequencies of soft sediments and determining the sediment thickness (Field and Jacob 1993; Lachet and Bard 1994; Lermo and Chavez-Garcia 1994; Mucciarelli 1998; Bindi et al. 2000; Parolai et al. 2010; Chopra et al. 2013). Through the Nakamura  $H/V$  spectral ratio method, the natural predominant frequencies of the soil of the study area can be revealed more accurately. Since the predominant frequency amplitude calculated with Nakamura  $H/V$  spectral ratio method is lower than that calculated from earthquake records, the amplification ( $H/V$ ) value obtained from Nakamura  $H/V$

✉ Nilgün Sayil  
sayil@ktu.edu.tr

<sup>1</sup> Department of Geophysics, Engineering Faculty, Karadeniz Technical University, 61080 Trabzon, Turkey

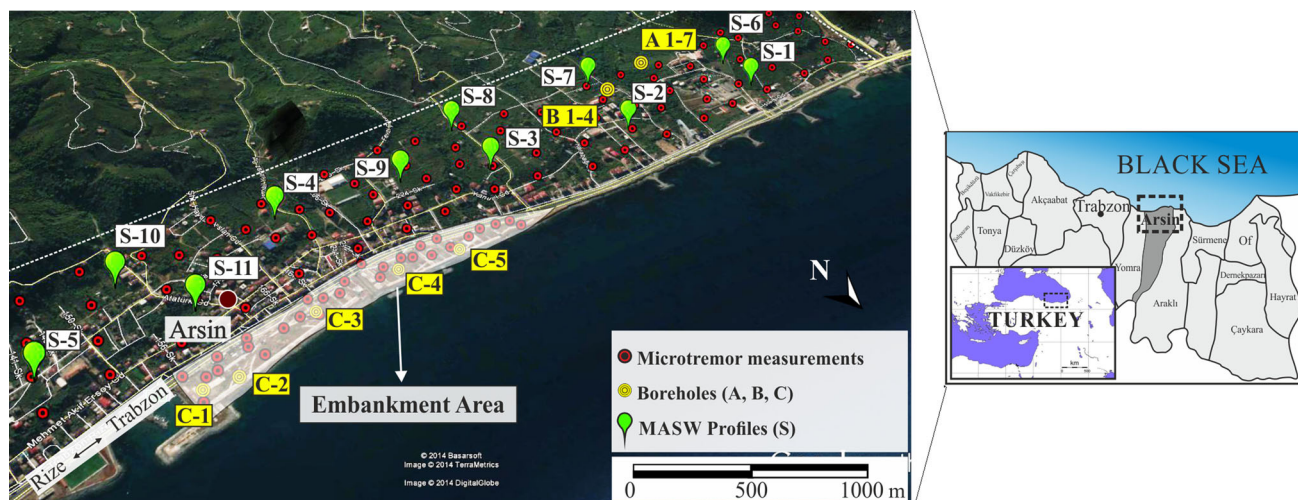
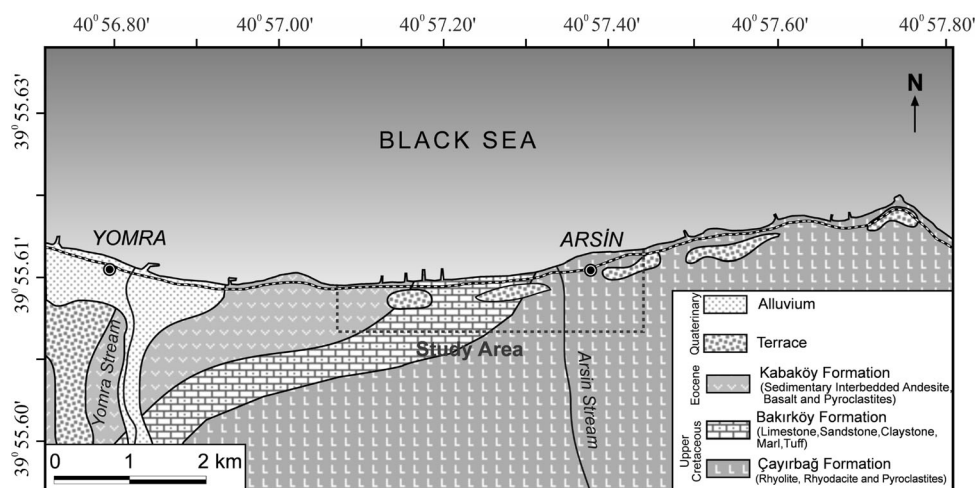


**Fig. 1** Locations of measurement points, profiles (S1–11) and borehole logs (A, B and C regions) in the study area

**Fig. 2** Geologic map of the study area and its environment [modified from Güven (1993)]



$V$  spectral ratio curves from microtremor records is not reliable (Bonilla et al. 1997; Bour et al. 1989; Lachet and Bard 1994).

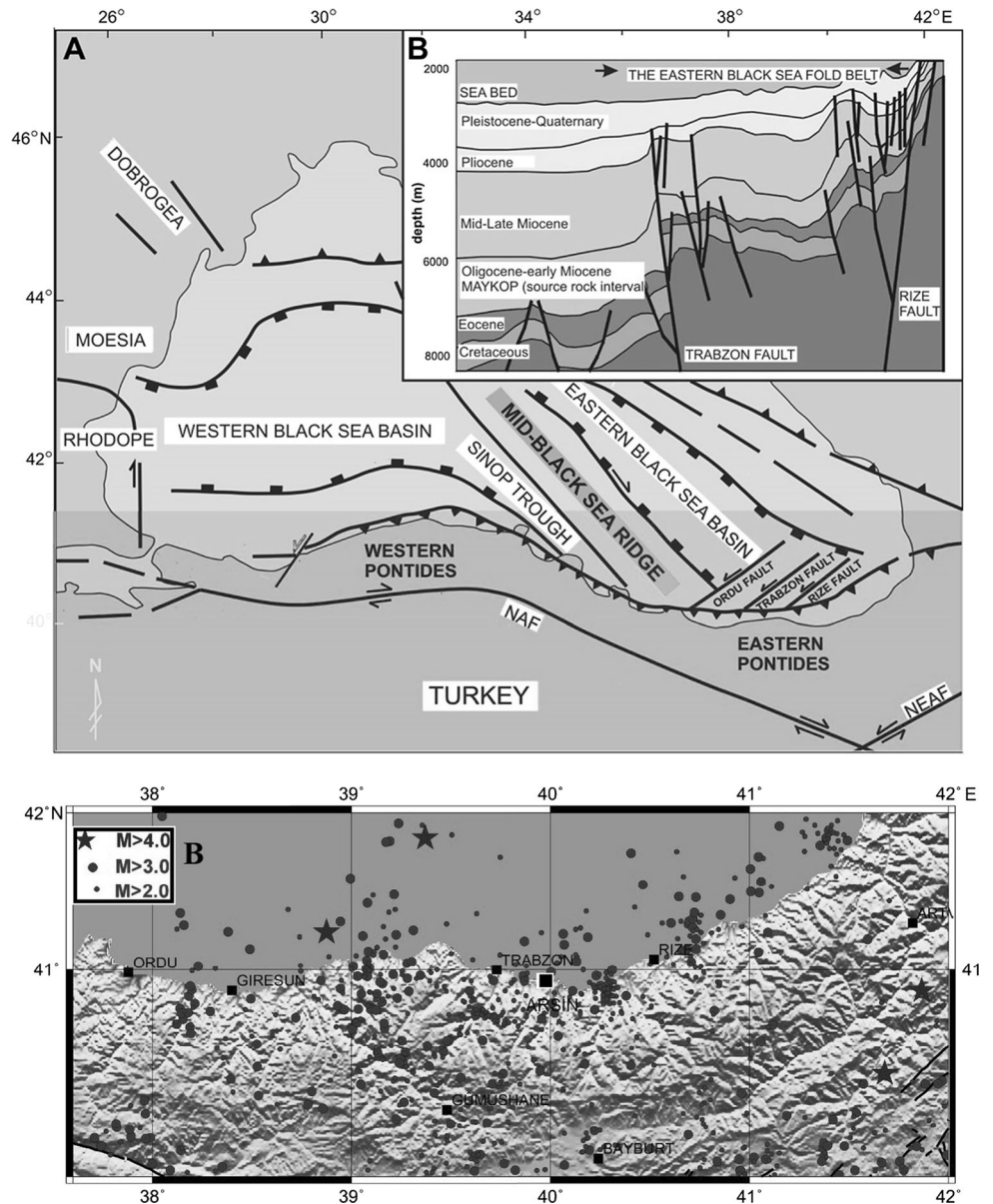
The aim of this study is to determine potential site effects in Arsin-Trabzon province of northern Turkey. The reasons for the selection of the study area are existence of active faults (NAF) producing major earthquakes and under the effect of the overthrust zone along the shoreline near this area, and it is planned to establish a new residential area by filling the sea. The soil dynamic characteristics in the study area have been determined by using active-source (MASW) and passive-source (single-station microtremor) surface wave methods. The soil predominant period ( $T_M$ ) and the  $H/V$  spectral ratio were obtained from single-station Nakamura  $H/V$  spectral ratio method. The shear-wave velocity ( $V_S$ ), the soil predominant period ( $T_R$ ), the bedrock depths and the soil amplification values according to three different methods [A (Midorikawa 1987),  $A^*$  (Medvedev

1965), AHSA (Borcherdt et al. 1991)] have been determined by means of MASW method in this study.

### Geological structure of the region

The study area covering approximately 3 km<sup>2</sup> land in Arsin-Trabzon (Fig. 1) involves the Cretaceous and Tertiary period units, and they are in sort from older to newer as Late Cretaceous Çayırbağ Formation, Late Cretaceous–Paleocene Bakırköy Formation, Eocene Kabaköy Formation, and Quaternary terrace set—alluvium (Güven 1993) (Fig. 2). As a result of these orogenic movements, different deformation structures have developed in Arsin-Trabzon being under the effects of Alpine orogenic movements, and the most important ones among them are the faulted structures. These structures indicate the vertical fault planes controlling the tectonic development of

**Fig. 3** **a** Tectonic map covering Black Sea and its environment [modified from Eyüboğlu et al. (2011) and TPAO/BP (1997)], **b** the earthquake activity of the region between 1990 and 2013 (Boğaziçi University, Kandilli Observatory and Earthquake Research Institute)



Trabzon and its surroundings in NE, NW and EW directions. Moreover, the presence of reverse and normal faults moving together with those faults indicates that the region is sometimes exposed to compression and tension stress (Keskin et al. 2011).

The presence of a reverse fault covering all the southern shoreline of Black Sea is known from previous studies, seismic researches of TPAO/BP (1997) in this region and actual researches (Kazmin et al. 1986; Nikishin et al. 2003; Eyüboğlu et al. 2011). Recent geological, geophysical and GPS data, and petroleum exploration offshore of Trabzon, Rize, and Hopa imply that an active collision system extends from Georgia into the eastern Black Sea shelf area along the Rize–Trabzon–Ordu line (Fig. 3a). The earthquake activity that has increased particularly in recent

period is explained with the presence of these reverse faults (Fig. 3b).

**Borehole logs in the study area**

In this study, the boreholes (Fig. 4) opened in three different zones of the study area by engineering companies (Adıgüzel 2012; Kurt 2008; Underground 2012). Three different zones of borehole logs are named with letters of A (7 pcs), B (4 pcs) and C (5 pcs) as shown in Fig. 1. The borehole logs in A and B regions are so close to each other. Thus, the locations of borehole logs in these regions are shown with the point symbols as “A1-7” and “B1-4” in Fig. 1. With the borehole logs, it has been defined that Bakırköy Formation

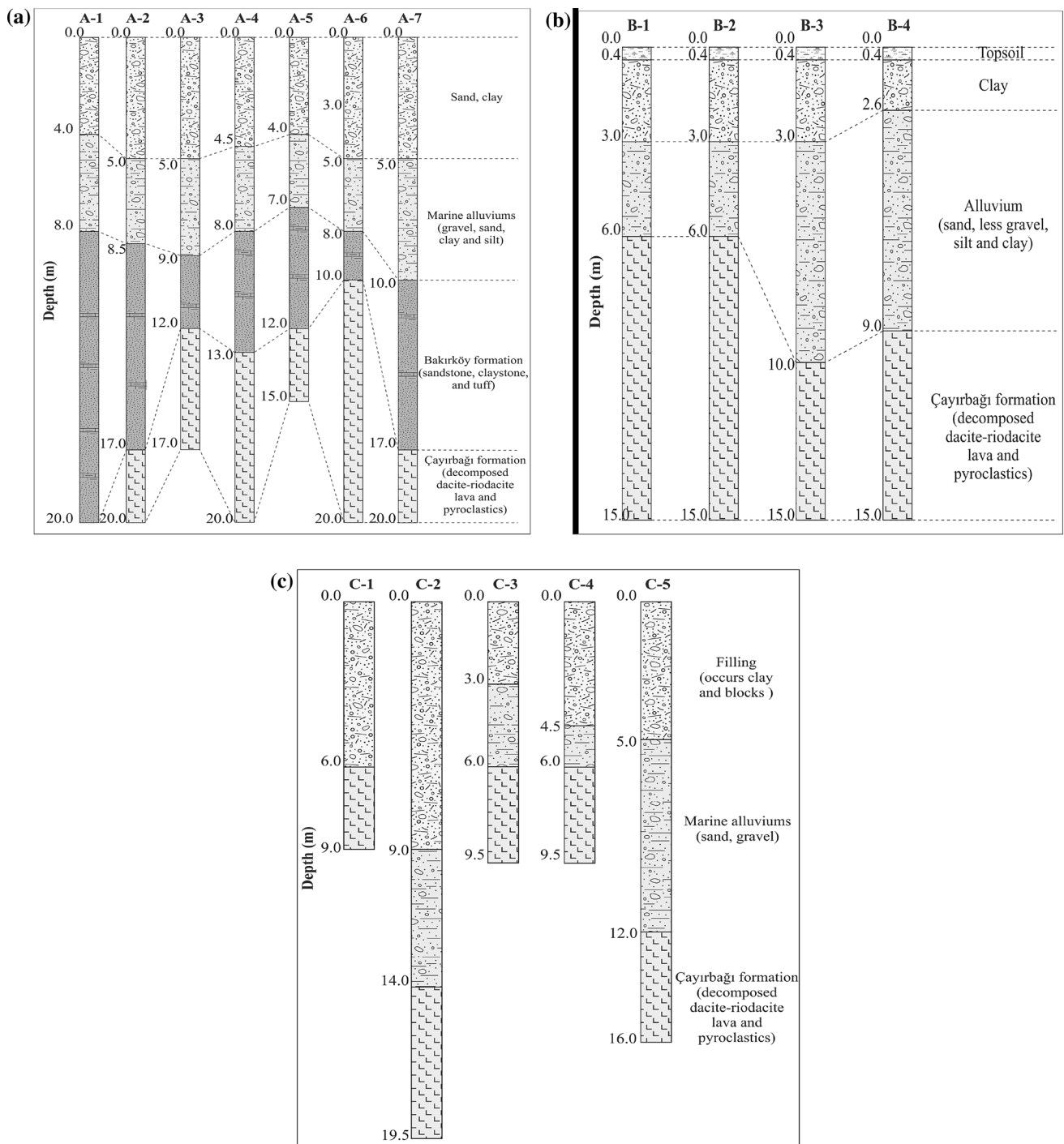


**Fig. 4** Borehole logs belonging to A, B and C regions which its locations are shown in Fig. 1 (Adıgüzel 2012; Kurt 2008; Underground 2012)

contained approximately 10 m alluvium unit, 5 m sandstone, clay stone, and limestone and Çayırbağı Formation contained 5 m dissociated rhyodacite lava and pyroclastic. It has also been determined the embankment of 3–5 m, approximately 5 m marine alluvium and Çayırbağı Formation in embankment area (Fig. 4).

### Geophysical field studies

The modeling of soil and its dynamic actions have been investigated by geophysical field studies. Within this scope, the single-station microtremor and MASW measurements have been performed and then evaluated.

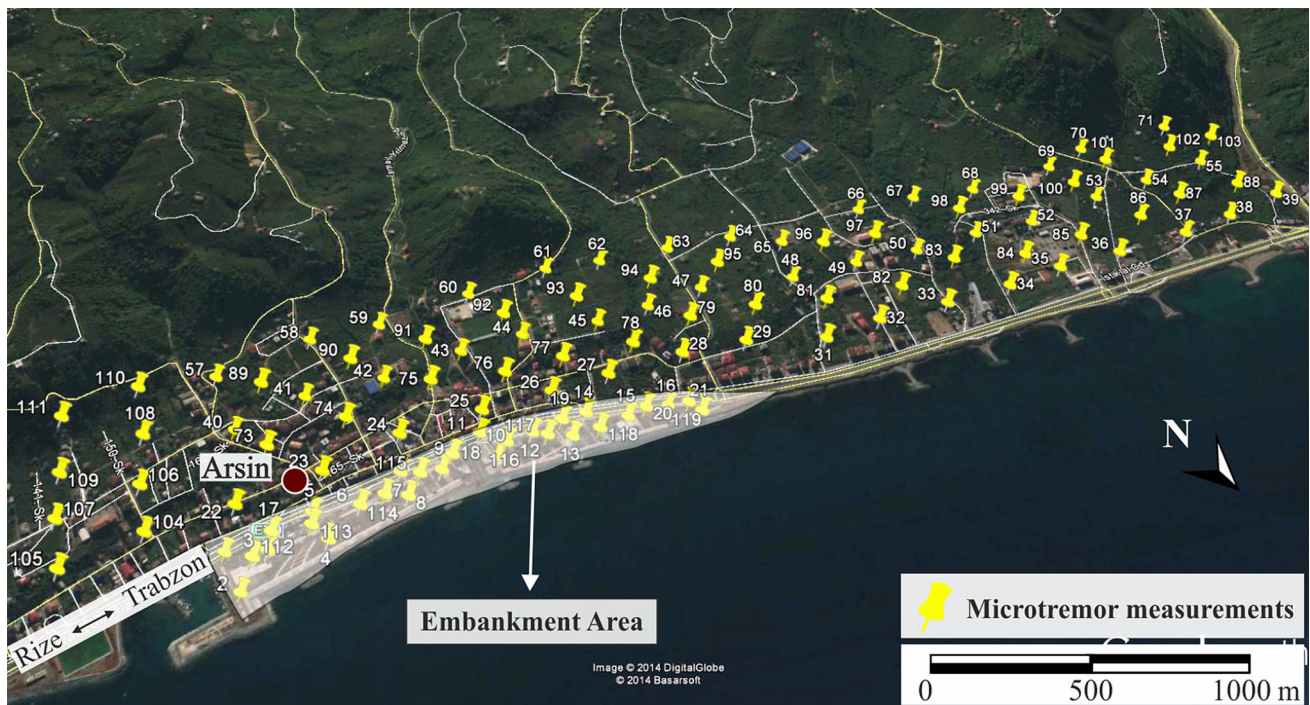


**Fig. 5** Spatial distribution of the microtremor measurements in the study area

**Single-station microtremor measurements**

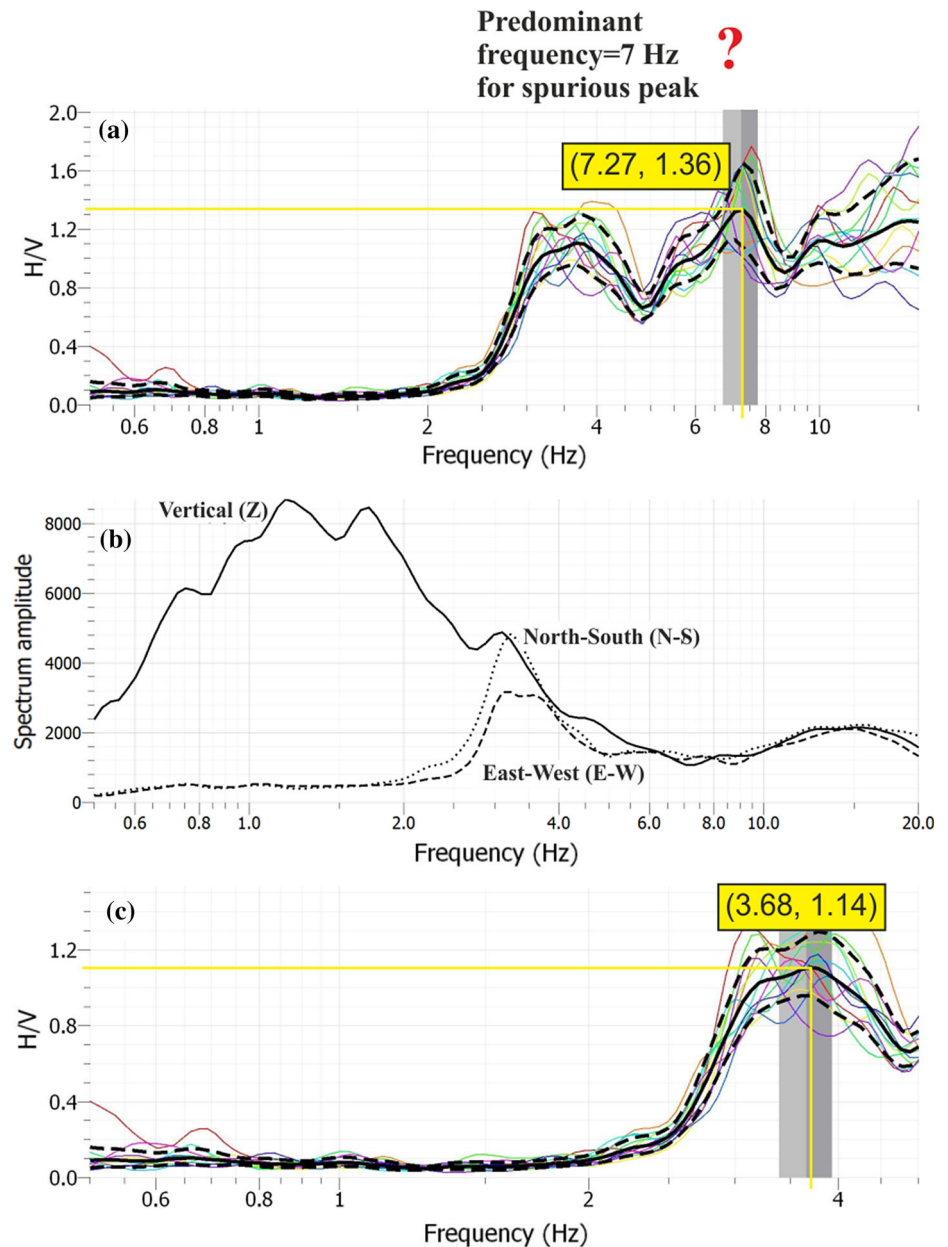
The study area covering approximately 3 km<sup>2</sup> of area, a total of 116 single-station microtremor measurements (29 of them in embankment area) have been performed (Fig. 5). The results have been confirmed by repeating the measurements under particularly different conditions (i.e., in daytime and meteorological). Although the locations of measurement points vary depending on the area conditions, they have been determined with 100 to 150-m interval, and the measurements have been taken with a portable, three-component digital output broadband seismometer (Guralp System CMG-6TD).

In order to obtain high-quality records, the technical rules determined for instrumental (the reliability and accuracy of digitizer–sensor couples) and experimental (the reliability of the results and rapidity of data collection) conditions within the scope of SESAME project of Europe (SESAME 2004; Chatelain et al. 2008; Guillier et al. 2008; Bard 2008) have been implemented. The recording equipment (especially the sensor) has been periodically tested by performing frequent recordings on a well-known site. Although the minimum record duration is 15 min, by monitoring the records from the computer, the recording durations have been extended up to 45 min in case of any environmental-origin corruptive effects.

The Nakamura *H/V* spectral ratio method (Nakamura 1989) has been implemented by evaluating the single-

station microtremor records with software (GEOPSY 1997). A series of processes have been applied to the raw data. The trend effect on records due to amplitude changes has been removed. Considering frequency range of microtremors, 0.5–20 Hz bandwidth Butterworth filter has been implemented to data. The recording has been divided into 25 s long windows after an automatized selection based on short-term average/long-term average (*STA/LTA*) ratio ( $0.2 < STA/STALTA.LTA < 2$ ). Even though the effect on *H/V* spectral ratio is negligible in appropriately long records, the disruptive effects (for example, the effects of local traffic) of the records have been removed from data according to  $STA/LTA < 2$ . It has been paid attention to that the number of selected windows is minimally 10 and the window length has been decreased down to 20 s in case of the number of windows decreased down from 10. The energy leakage has been prevented by applying the 5 % cosine window to the data in this phase. Fourier amplitude spectrums have been obtained for each of windows, and each of components and the spectra has been smoothed applying the Konno and Ohmachi window (Konno and Ohmachi 1998) by selecting  $b = 40$ . So, the *H/V* spectral ratios have been calculated for each of windows and each of frequencies by calculating the geometrical average of north–south and east–west components. In order to calculate an average *H/V* curve according to *H/V* spectral ratio at 95 % confidence interval, the average of spectral ratios determined from all the time windows has been calculated.

**Fig. 6 a** Spurious peak at 7.27 Hz in average  $H/V$  curve calculated with Nakamura  $H/V$  spectral ratio methods (*black line*), **b** amplitude spectrums of three-component microtremor records, **c** true predominant frequency of 3.68 Hz and  $H/V$  ratio of 1.14 were determined accurately by considering the amplitude spectrum. The *colored lines* represent the  $H/V$  curves calculated for each of windows, and the *dashed lines* represent the  $\pm 1$  standard deviation



From the aspect of soil characteristics, the first point to pay attention for an appropriate interpretation of  $H/V$  curves is to determine the  $H/V$  peaks (because of impulsive or anthropic reasons in local zones) by designing the  $H/V$  along different horizontal directions. Accordingly, those windows have been removed by determining the disruptive directional effects, and the average  $H/V$  spectral ratio has been calculated again. It has been observed that this process has not affected the  $H/V$  spectral ratio and has decreased the variability of confidence level (Picozzi et al. 2009). In second step, the SESAME criteria (SESAME 2004) have been implemented in interpretation of  $H/V$  curves. The possible pseudo-originated peaks (further

sharpening sharp peaks in all the components of spectrum by descending smoothing) or the peaks occurring under the effect of low frequency (wind, bad soil-sensor coupling, etc.) have been determined, and it has been paid attention to resolve the broad or multiple peaks (occurring as a result of changed smoothing parameters). In all uncertain cases, the measurements have been repeated. The amplitude spectrums of three components have been taken into account in distinguishing the spurious peaks. For example, in order to make a decision about which one of two maximum (3.68 and 7.27 Hz frequency) peaks seen in  $H/V$  graphic in Fig. 6a represents the true predominant period and  $H/V$  spectral ratio, the amplitude spectrums have been

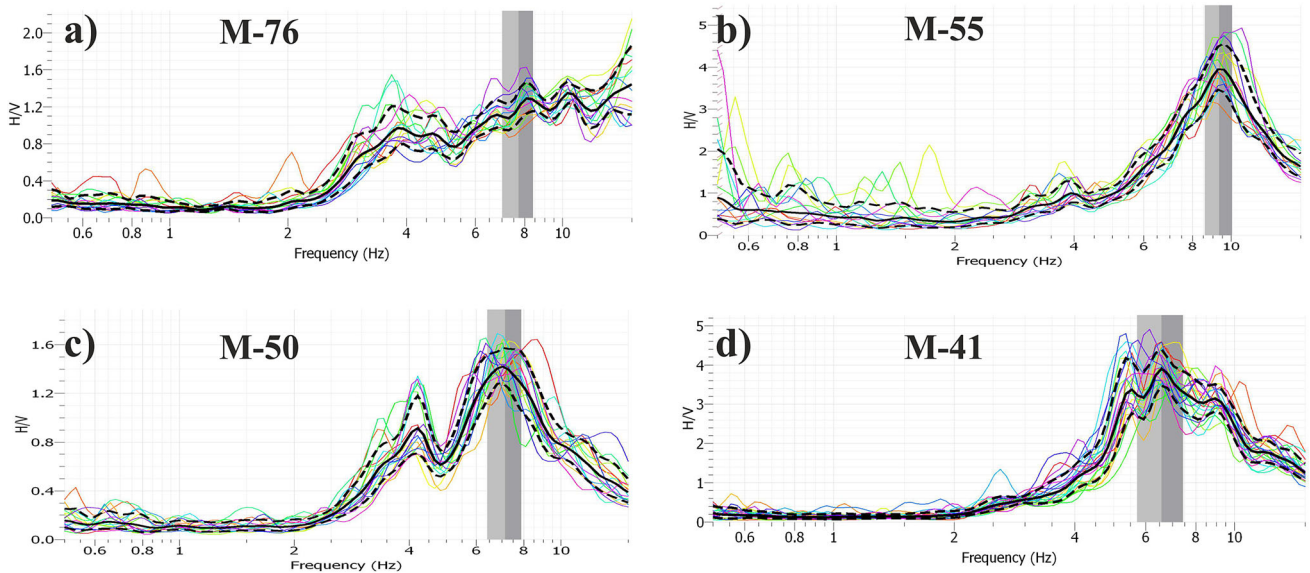


**Fig. 7** Average  $H/V$  spectral ratio graphics obtained for 4 points in Fig. 5. Example of **a** flat peak, **b** single peak, **c** double peaks and **d** multi-peak  $H/V$  curves. Average  $H/V$  curves (black line),  $\pm 1$

standard deviation (dashed line) and  $H/V$  graphics for each of selected windows (colored lines)

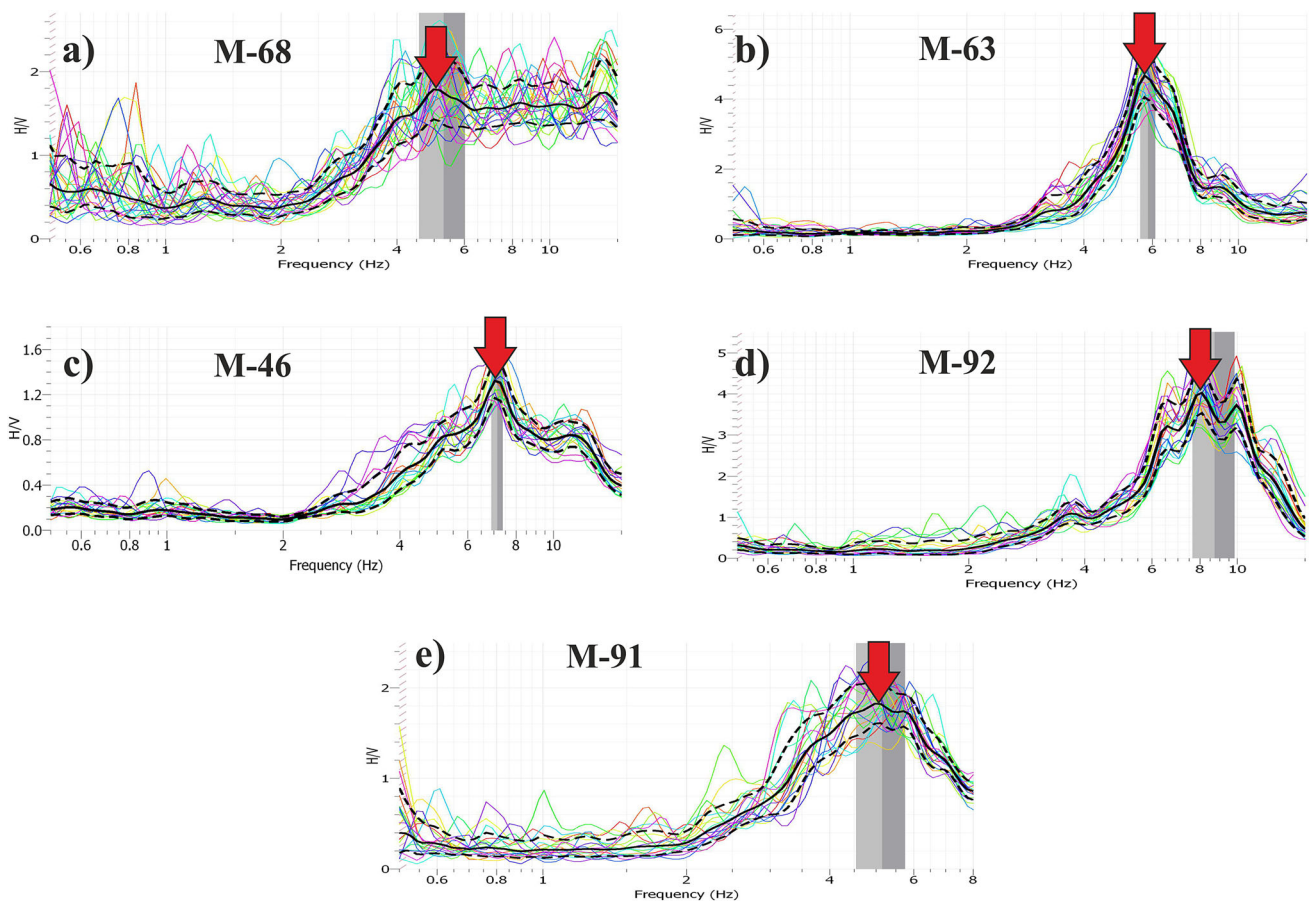


**Fig. 8** Average  $H/V$  spectral ratio graphics obtained for 5 points in Fig. 5. Colored lines represent the  $H/V$  graphics calculated for selected windows, dashed lines represent  $\pm 1$  standard deviation

value, and red arrow sign indicates the predominant frequency and  $H/V$  value obtained from Nakamura  $H/V$  spectral ratio method

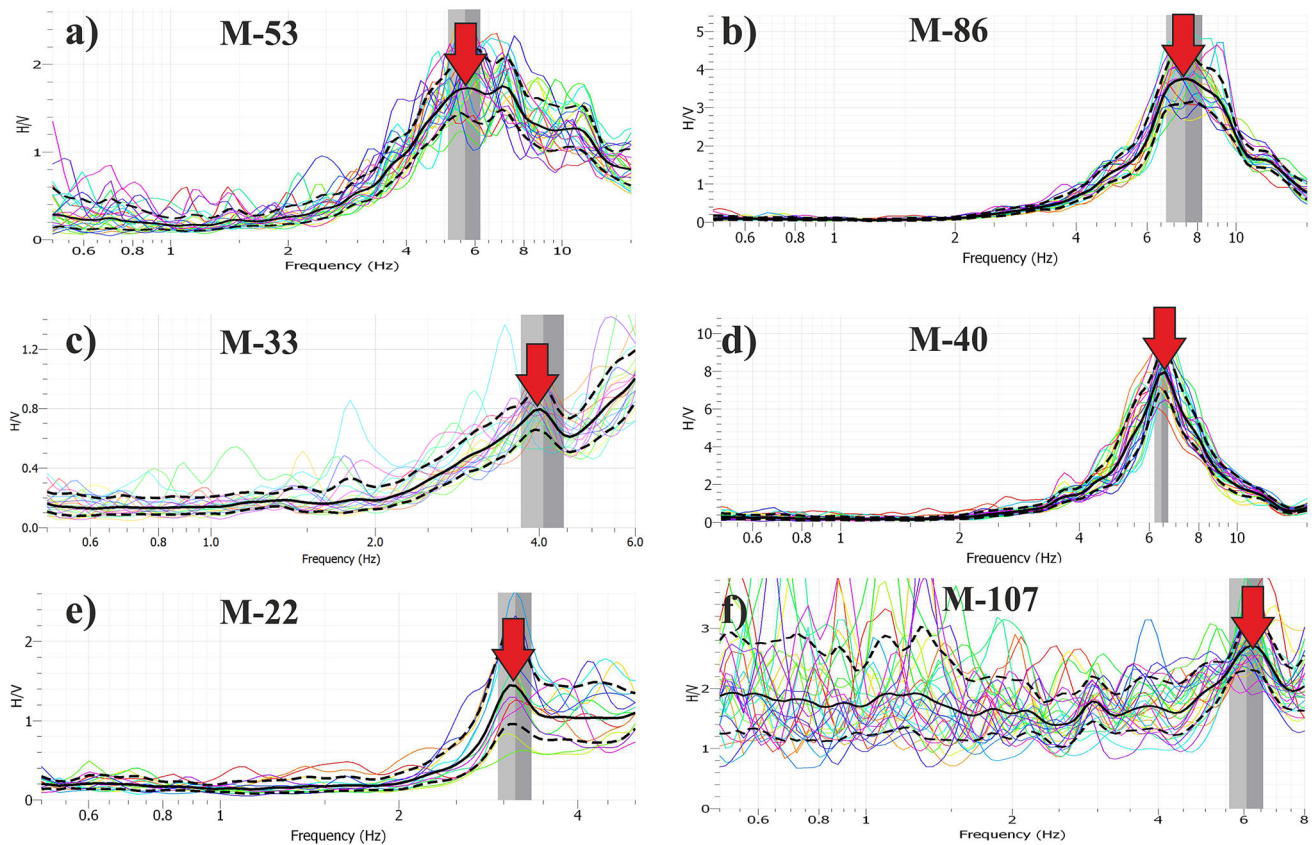


**Fig. 9** Average  $H/V$  spectral ratio graphics obtained for 6 points in Fig. 5. Colored lines represent the  $H/V$  graphics calculated for selected windows, dashed lines represent  $\pm 1$  standard deviation

investigated. When amplitude spectrums (Fig. 6b) of three components are evaluated, it can be seen that there occurs a spurious peak because the minimum value of the vertical component falls into this frequency even if the real vertical components do not peak around 7.27 Hz. Hence, the peak giving the true predominant period and  $H/V$  value is in 3.68 Hz frequency (Fig. 6c).

The calculated  $H/V$  curves also represent the soil structure. The flat  $H/V$  curves represent the soil structure around the outcropping rock units where there is no clear impedance contrast in deeper points. In case of only a single peak, the frequency corresponding to this peak gives the fundamental resonance frequency of the soil. In case of two or more peaks with frequencies higher than fundamental frequency, they have been interpreted as further natural resonance frequencies related to one or more shallow impedance contrasts at depth, and not as higher mode resonances, which should be uneven multiples of fundamental frequency (SESAME 2004; Picozzi et al. 2009; D'Amico et al. 2008). The peak with highest amplitude gives the predominant frequency. The most typical  $H/V$  curves are shown in Fig. 7. A couple of  $H/V$

value, and red arrow sign indicates the predominant frequency and  $H/V$  value obtained from Nakamura  $H/V$  spectral ratio method

$V$  curves calculated from microtremor measurements which locations are shown in Fig. 5 have been presented in Figs. 8, 9 and 10, and the numeric values are given in Table 1.

### MASW measurements and evaluations

The active-source MASW method has been implemented on selected 11 profiles (as shown in Fig. 1) with 24-channel seismograph (PASI 16-S-24U) and 4.5 Hz vertical geophones. Ten kilograms of hammer was used as source. The profile lengths have been selected as 84 m (S-1, S-6) and 61 m (other profiles) depending on area conditions (Fig. 1). The parameter set used during the measurements has been selected according to the procedure as defined by (Park et al. 2002). It has been tried to obtain the best results by choosing the distance of source from the first geophone (offset) to be 15, 10 and 5 m in all the profiles, respectively. The recording length and the sampling interval have been selected as 1024 and 1 ms, respectively. In order to improve the data quality, 5 vertical stacks have been performed in all the profiles.



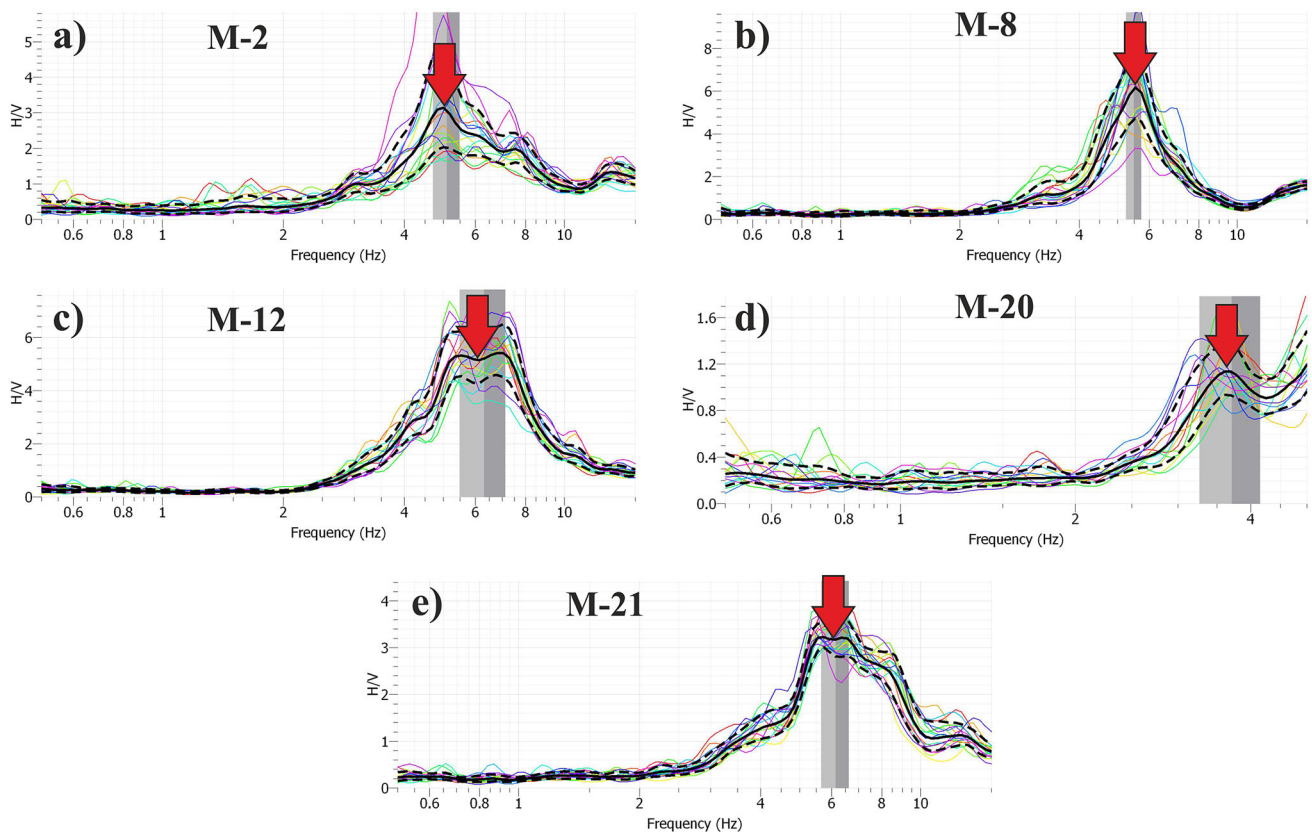


**Fig. 10** Average *H/V* spectral ratio graphics obtained for 5 points on embankment area in Fig. 5. Colored lines represent the *H/V* graphics calculated for selected windows, dashed lines represent  $\pm 1$  standard

deviation value, and red arrow sign indicates the predominant frequency and *H/V* value obtained from Nakamura *H/V* spectral ratio method

**Table 1** Predominant period, *H/V* values and the number of used windows obtained by implementing Nakamura *H/V* spectral ratio method on microtremor data which locations are shown in Fig. 5

Microtremor no	M-68	M-63	M-46	M-92	M-91	M-53	M-86	M-33	M-40	M-22	M-107	M-2	M-8	M-12	M-20	M-21
<i>H/V</i> value	3.18	2.93	1.32	3.80	1.80	1.70	3.69	1.91	7.80	1.44	2.69	3.10	6.15	5.30	1.14	3.21
Pre. period (s)	0.13	0.13	0.14	0.13	0.21	0.20	0.14	0.13	0.15	0.32	0.16	0.20	0.18	0.18	0.28	0.17
Num. of Win.	25	24	17	19	19	24	13	11	25	13	28	18	18	16	14	17

The data were evaluated with software (SeisImager/Pickwin 2014). In data process implemented on taken MASW measurements (Fig. 11a), firstly the phase velocity–frequency graphic has been obtained (Fig. 11b). The dispersion curves have been obtained by marking the highest amplitudes in phase velocity–frequency image (Fig. 11c). Because it involves optimum data about both of shallow and deep layers, the fundamental mode has been used while obtaining observational dispersion curve (Fig. 11d). Afterward, the inversion has been made and the calculated theoretical dispersion curve has been overlaid with obtained observational dispersion curve by using damped least-squares technique (Levenberg 1944; Marquardt 1963), (Fig. 11e). The 1D structure of the shear-wave velocity has been obtained from inversion of this curve (Fig. 11f).

### Results and discussion

The predominant period ( $T_M$ ) contour map has been created by Nakamura *H/V* spectral ratio method and two cross sections (AA' and BB') selected for comparing the soil parameters (Fig. 12). The predominant periods change mostly between 0.1 and 0.2 s, but they reach up to 0.37 s and the average period is 0.17 s in the city center. These values correspond with soil class “I” according to Kanai and Tanaka classification (Kanai and Tanaka 1961), and geologically with “Rock, stiff sandy gravel units.” The average predominant period is 0.22 s, and the highest period is 0.33 s in the embankment area. That means the soil class of the embankment area is “II” according to Kanai and Tanaka classification (Kanai and Tanaka 1961)

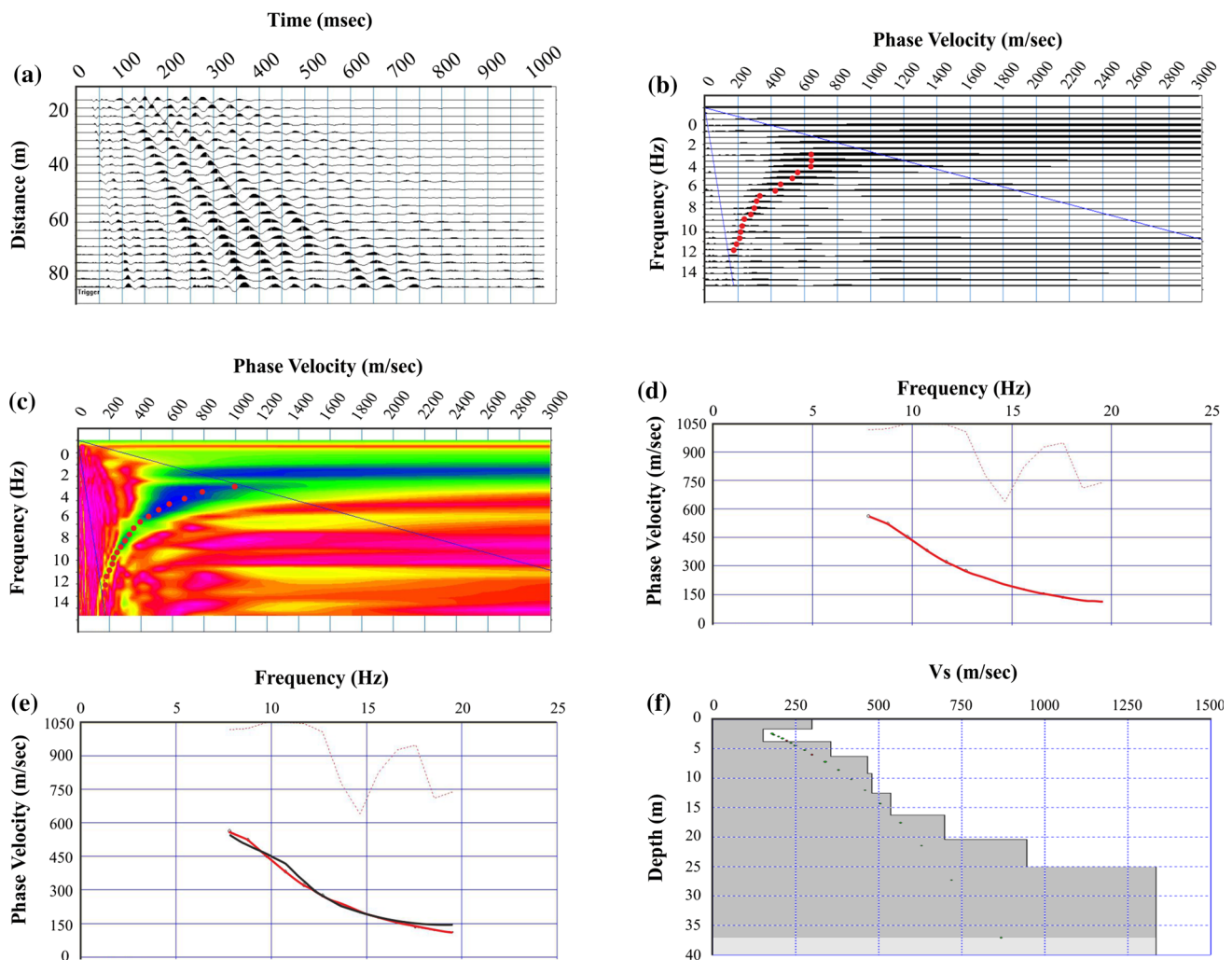


**Fig. 11** **a** A sample MASW series used in study, **b** phase velocity–frequency image where the highest amplitudes are signed, the *slant lines* represent confidence interval, **c** phase velocity–frequency image where the highest amplitudes are colored, the *slant lines* represent

confidence interval, **d** measured dispersion curve, *light colored curve on top* shows data quality, **e** overlay of measured and calculated (*dark colored curve*) dispersion curves, *light colored curve on top* shows data quality, **f** 1D shear-wave velocity structure ( $V_S$ )

and geologically correspond with “sandy gravel, marine alluviums consist of stiff clay with sand or thicknesses of 5 m or more thick gravelly alluvium.”

$H/V$  spectral ratios were calculated, and the contour map was created (Fig. 13). The obtained  $H/V$  ratios vary between 1 and 8. This ratio is expected to be low in stiff soil and to be high in soft soil. The higher  $H/V$  spectral ratios are in eastern part of the study area, while lower  $H/V$  ratios are in western part of the area as well as the predominant periods. Regarding to  $H/V$  spectral ratios in embankment area, it can be said that they are relatively higher than the rest of the study area.

The  $V_S$  values obtained by using MASW method vary between 162 and 1376 m/s. As a result of measurements taken from 11 profiles (S1–S11, Fig. 13), the 1D velocity structures were obtained (Fig. 14). The results show that

the research depths vary between 13 and 38 m. The bedrock depth for each of profiles has been determined by 1D velocity structures, which are obtained using these velocity and depth information. The bedrock depth of the study area is determined as approximately 10–15 m with considering all of the depth information. Also, it can be seen that the 1D velocity structures are in harmony with borehole logs, as shown in Fig. 4.

The  $V_{S30}$  velocities were calculated by using obtained  $V_S$  values, and the contour map was prepared. The  $V_{S30}$  values vary between 428 and 817 m/s. While the velocities decrease in western part of the study area, high velocities are observed in central parts of the study area (Fig. 15). Two different soil classifications (NEHRP: National Earthquake Hazards Reduction Program and Eurocode 8) were performed by using  $V_{S30}$  value, since this parameter is

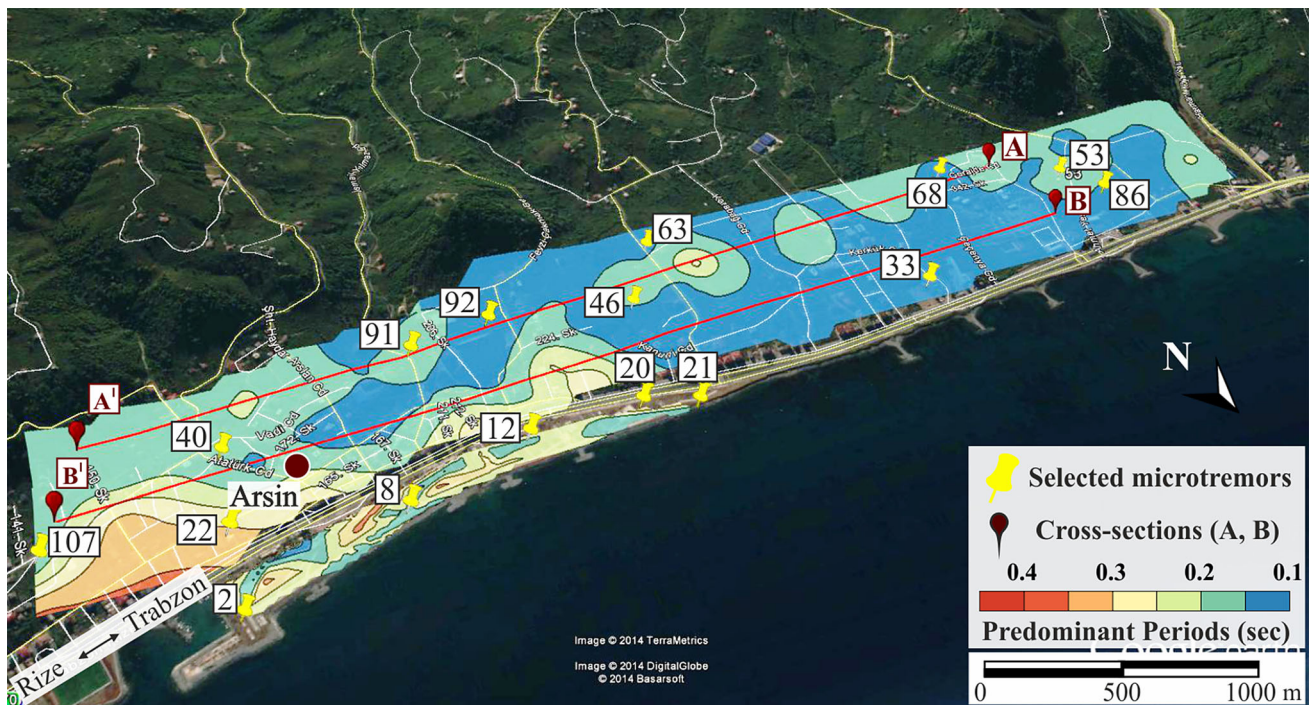


**Fig. 12** Soil predominant period ( $T_M$ ) contour map obtained by Nakamura  $H/V$  spectral method on single-station microtremor data collected from the study area

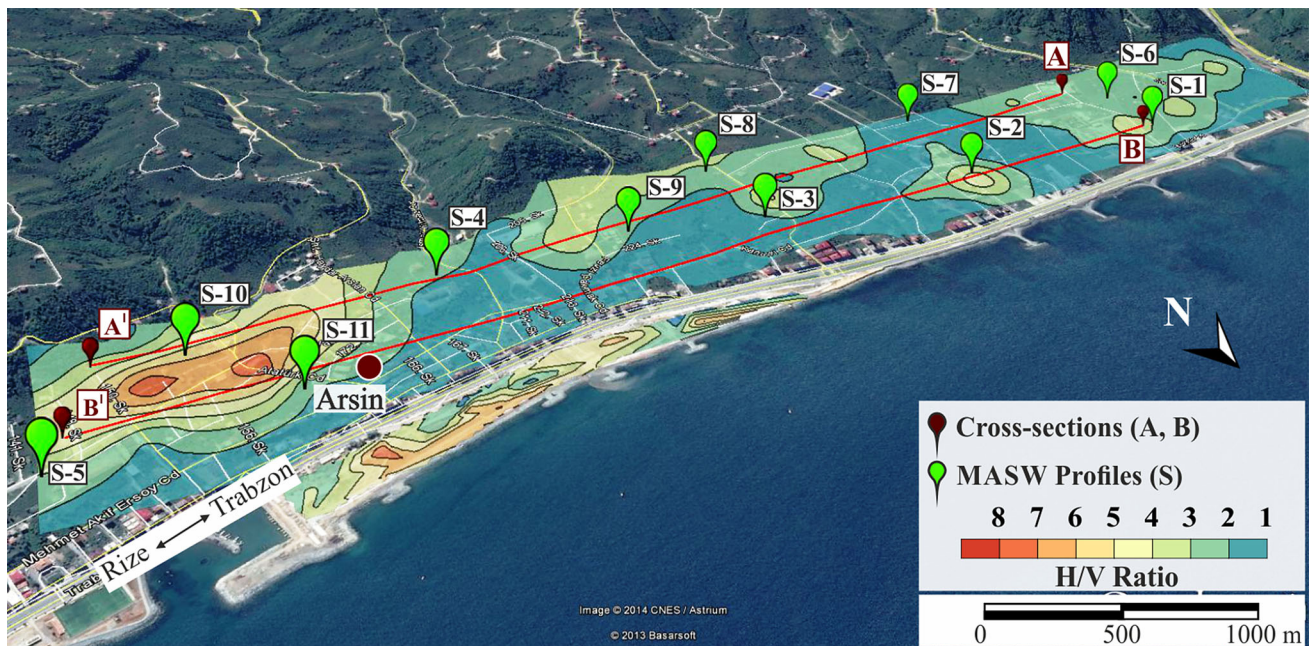


**Fig. 13**  $H/V$  spectral ratio contour map obtained by Nakamura  $H/V$  spectral ratio method in the study area

very important for solving the engineering problems (Table 2). As a result of the classification, the study area was found to be mostly C (NEHRP) and B (Eurocode 8) classes. Even though soil classifications are different, C and B classes represent similar geological properties and

soil density softness values. The average shear-wave velocity of 10 m ( $V_{S10}$ ) by considering base depth of buildings has been calculated from  $V_S$  values (Fig. 16). The bedrock depths were determined according to 1D velocity structures obtained for each of profiles. The layer where

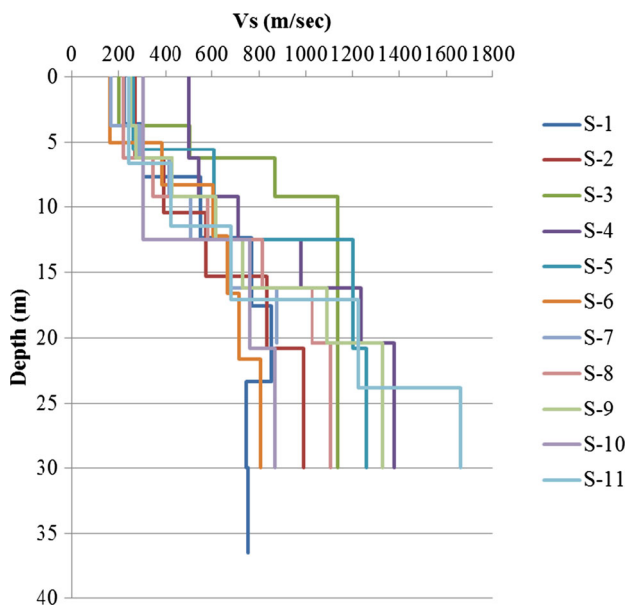


**Fig. 14** 1D shear-wave velocity ( $V_s$ ) structures obtained from MASW method for all profiles

shear-wave velocities higher than 760 m/s named as seismic base represents the bedrock depth.

The soil predominant periods (MASW:  $T_R$ ) were calculated by MASW method according to Kanai (1983), and the predominant period contour map was prepared

**Table 2** NEHRP and Eurocode 8 classifications, according to  $V_{S30}$  values which were obtained from profiles in the study area

Cross sections	Profiles	$V_{S30}$ (m/s)	Soil classification	
			NEHRP	Eurocode 8
AA'	S-6	428.87	C	B
	S-7	460.41	C	B
	S-8	499.06	C	B
	S-9	570.71	C	B
	S-4	817.06	B'	A
	S-10	482.77	C	B
BB'	S-1	469.50	C	B
	S-2	515.15	C	B
	S-3	662.67	C	B
	S-11	531.74	C	B
	S-5	667.90	C	B

A, rock or other rock-like formations ( $V_{S30} > 800$  m/s); B, very tight sand, gravel or very stiff clays ( $V_{S30}$  360–800 m/s); B', rock ( $V_{S30}$  760–1500 m/s); C, very tight/hard or soft rock ( $V_{S30}$  360–760 m/s)

(Fig. 17). The obtained predominant period values ( $T_R$ ) vary between 0.1 and 0.36 s, and it is observed that they are in harmony with predominant period values ( $T_M$ ; 0.1–0.37 s) obtained from single-station method. It can be seen that predominant period values generally vary between 0.1 and 0.2 s from  $T_R$  contour map, but these

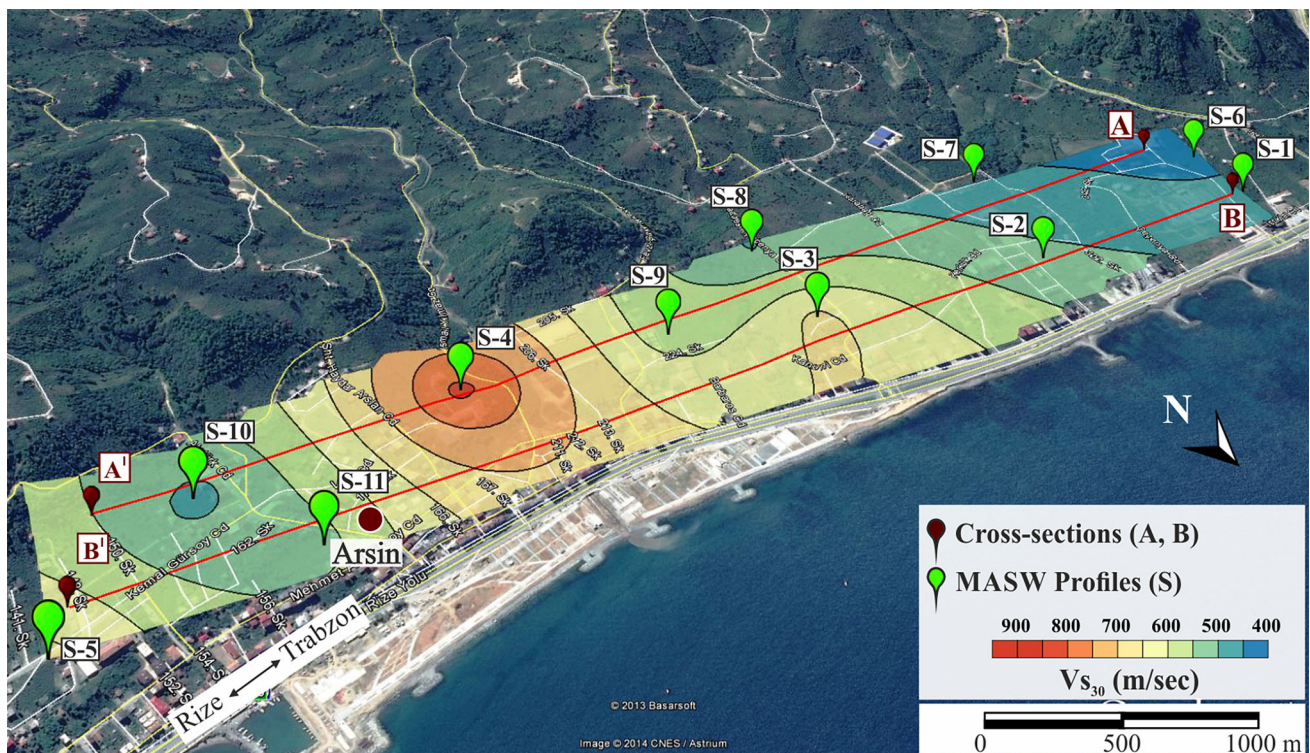


**Fig. 15**  $V_{S30}$  contour map of the study area

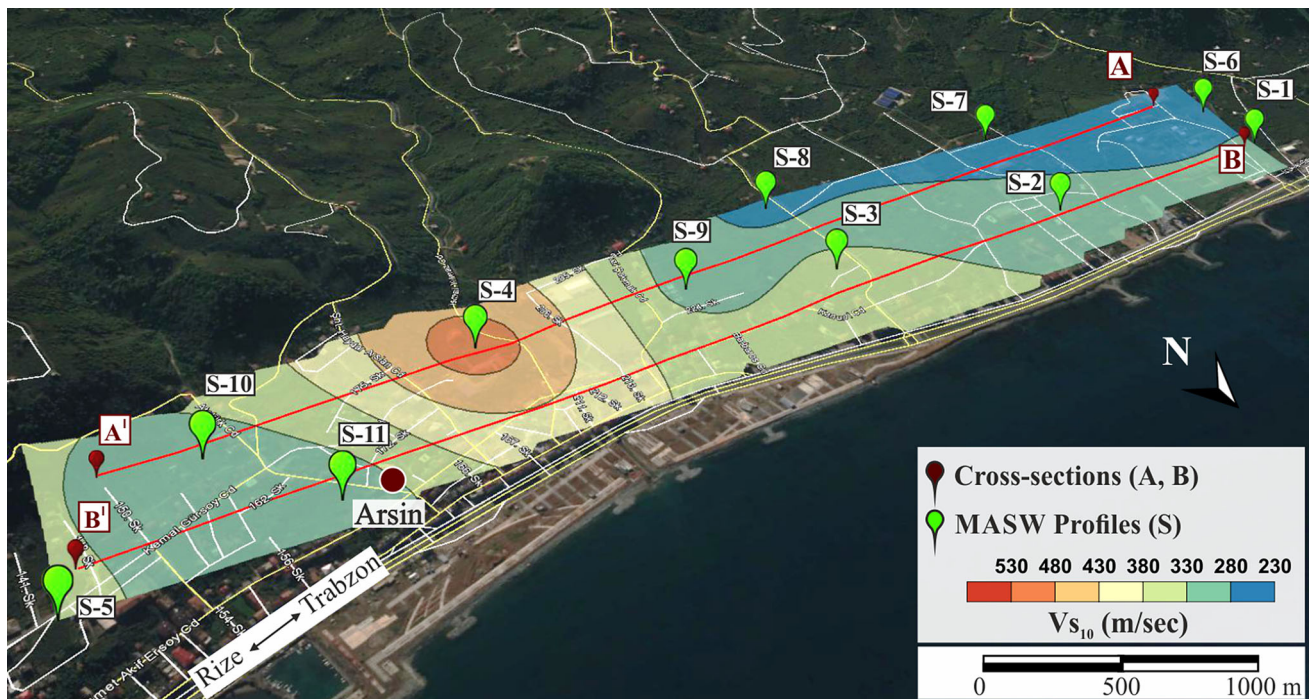


Fig. 16  $V_{S10}$  contour map of the study area

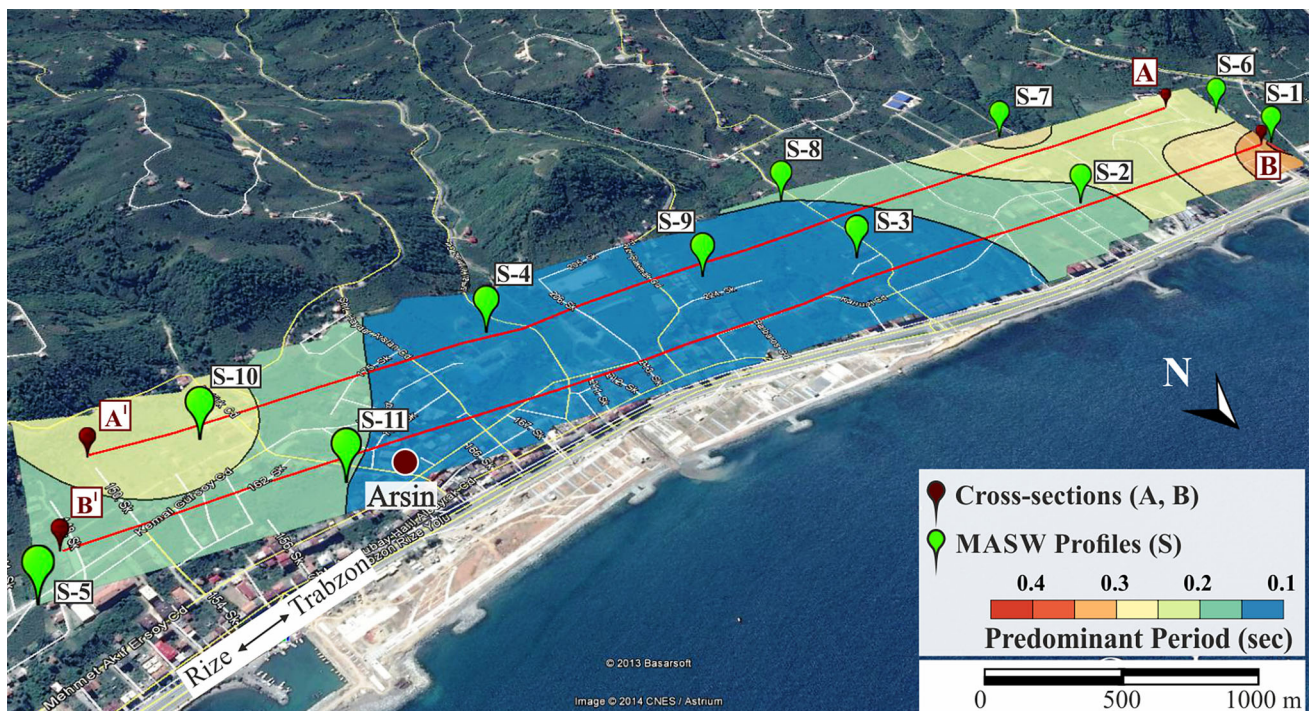


Fig. 17 Soil predominant period contour map obtained from MASW method

values reach up to 0.36 s by increasing in eastern and western parts of the study area. Based on the acceptance that each of stages in buildings has 0.1 s of period,

resonance could be occur in 1–4 storey buildings according to  $T_R$  and  $T_M$  values. That is why, the risk should be taken into account during the building design. The soil

**Table 3** Amplification ( $A$ , AHSA,  $A^*$ ) values calculated according to (Midorikawa 1987; Borchardt et al. 1991; Medvedev 1965)

Cross sections	Profiles	$V_{S30}$ (m/s)	$A$	AHSA	$A^*$
AA'	S-6	428.87	1.79	1.63	1.52
	S-7	460.41	1.71	1.52	1.25
	S-8	499.06	1.63	1.40	2.30
	S-9	570.71	1.50	1.22	2.16
	S-4	817.06	1.21	0.85	1.34
	S-10	482.77	1.66	1.44	2.40
BB'	S-1	469.50	1.69	1.49	2.08
	S-2	515.15	1.60	1.35	1.95
	S-3	662.67	1.37	1.05	2.67
	S-11	531.74	1.57	1.31	2.70
	S-5	667.90	1.37	1.04	2.79
Average amplification			1.56	1.30	2.10

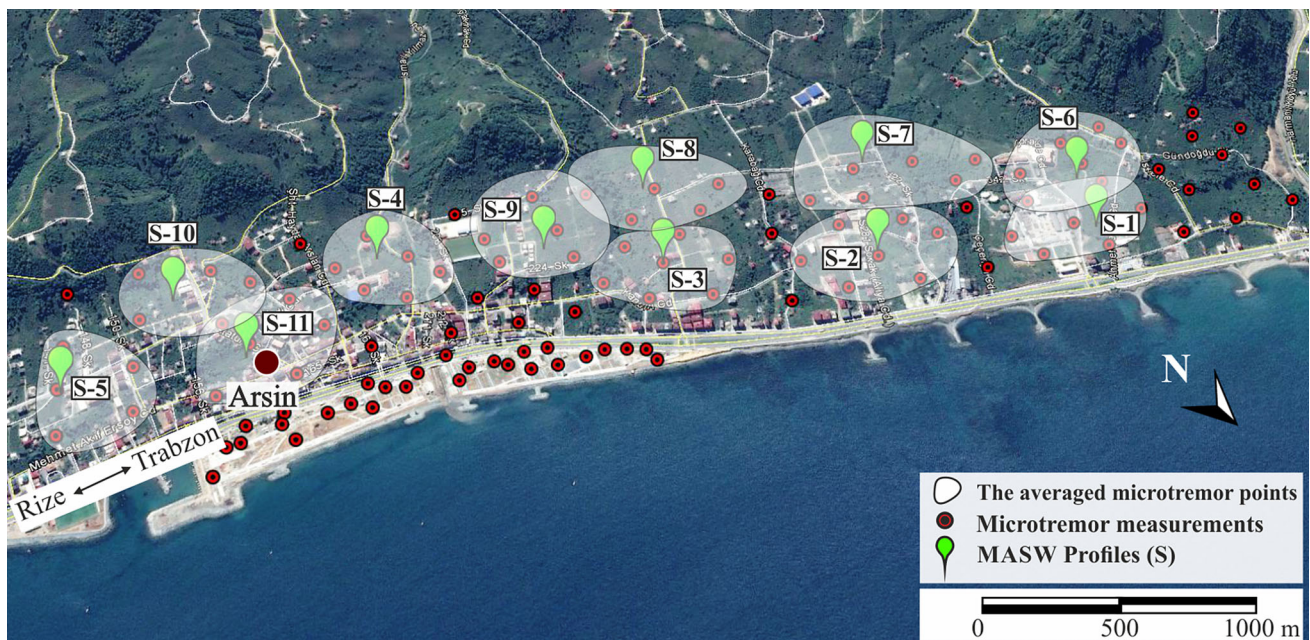
$A$ , relative amplification factor to maximum ground velocity ( $A = 68 (V_{S30} - 0.6, V_{S30} < 1100 \text{ m/s})$ ; AHSA, average horizontal spectral amplification in the range of 0.4–2.0 s period (AHSA =  $700/V_{S30}$ , for weak motion);  $A^*$ : Amplification factor,  $A^* = 1.67 \ln(\rho_0 V_{S0} / \rho_1 V_{S1})$ ;  $\rho = 0.44V_S^{0.25}$ ,  $\rho$ ; relative bulk density;  $V_S$ ; S-wave velocity

amplifications were calculated with three different methods based on  $V_{S30}$  and acoustic impedance (Keçeli 1996). The average amplification values were found to be 1.56 for  $A$  (Midorikawa 1987), 2.10 for  $A^*$  (Medvedev 1965) and 1.30 for AHSA (Borchardt et al. 1991) (Table 3).

In order to compare the results obtained from single-station microtremor and MASW method, 5–7

microtremor measurement points were selected around the MASW profiles (Fig. 18). The average of predominant periods ( $T_{MAve}$ ) obtained from single-station microtremor method and the predominant periods obtained from the MASW profiles ( $T_R$ ) are given in Table 4. In Table 5, the average of  $H/V$  spectral ratios ( $H/V_{Ave}$ ) obtained from single-station microtremor method and amplitudes calculated from MASW profiles according to the three different methods ( $A$ , AHSA,  $A^*$ ) were shown. Thus, differences between the results obtained from single-station microtremor and MASW method have been indicated.

Aiming to compare changes of  $V_{S30}$  and  $V_{S10}$  velocities, predominant periods ( $T_M$ ,  $T_R$ ), amplification ( $A$ ,  $A^*$ , AHSA) and  $H/V$  spectral ratios along AA' and BB' cross sections, the graphics were prepared (Figs. 19 and 20). The highest  $V_{S30}$  value has been found around the S-4 profile, and this value generally changes between 500 and 600 m/s. The  $V_{S10}$  values in the cross section AA' (Fig. 19a) are full harmony with  $V_{S30}$  values, but in cross section BB' (Fig. 20a) are partially harmonious. It is seen that the bedrock depth obtained by MASW method (Park et al. 2002) has been found between 10 and 15 m (Figs. 19b and 20b). Even if a complete overlap is not observed in  $T_R$  and  $T_M$  curves, these values are in harmony according to interval of the predominant period values ( $T_R$ : 0.1–0.37 s,  $T_M$ : 0.1–0.36 s), (Figs. 19c and 20c). The  $H/V$  spectral ratio and three different amplifications ( $A$ ,  $A^*$ , AHSA) are shown in Figs. 19d and 20d. It is seen that  $A$ ,  $A^*$  and

**Fig. 18** Measurement points (5–7 pcs) selected around both of cross sections for comparison the results

**Table 4** Average predominant periods ( $T_{MAve}$ ) obtained from single-station microtremor method (selected 5–7 pcs in Fig. 18) and predominant periods ( $T_R$ ) obtained from MASW method

	S-1	S-2	S-3	S-4	S-5	S-6	S-7	S-8	S-9	S-10	S-11
$T_M$ (s)	0.15	0.14	0.12	0.14	0.34	0.14	0.11	0.16	0.14	0.15	0.32
	0.13	0.13	0.14	0.13	0.37	0.20	0.15	0.11	0.14	0.17	0.28
	0.14	0.15	0.14	0.11	0.34	0.18	0.14	0.17	0.14	0.22	0.15
	0.20	0.14	0.12	0.13	0.16	0.18	0.17	0.20	0.13	0.15	0.16
	0.14	0.13	0.14	0.17	0.17	0.16	0.21	0.27	0.13	0.18	0.14
	0.11	0.13	0.14	0.21		0.13	0.13		0.15		0.13
$T_{MAve}$ (s)	0.14	0.14	0.13	0.15	0.28	0.16	0.15	0.18	0.14	0.17	0.20
$T_R$ (s)	0.36	0.17	0.11	0.10	0.16	0.20	0.27	0.16	0.15	0.23	0.15

**Table 5** Comparison of average  $H/V$  ratio ( $H/V_{Ave}$ ) obtained from single-station microtremor method (selected 5–7 pcs in Fig. 18) with average amplifications ( $A^*$ ,  $A$ , AHSA) obtained from MASW method

	S-1	S-2	S-3	S-4	S-5	S-6	S-7	S-8	S-9	S-10	S-11
$H/V$	1.50	1.39	1.05	1.63	1.60	2.00	1.13	3.17	2.85	7.80	1.44
	1.72	1.91	1.00	1.28	1.69	1.70	1.76	2.93	1.00	4.01	1.48
	2.00	1.60	1.32	2.60	1.90	2.11	3.18	2.72	3.29	6.16	7.80
	1.70	1.15	4.40	1.40	2.70	2.13	1.26	1.04	3.17	8.30	3.88
	2.10	2.20	1.55	2.24	5.23	2.35	2.20	1.70	3.80	2.00	2.20
	3.83	5.15	1.44	1.80		3.00	2.00		2.13		2.07
$H/V_{Ave}$	3.69	1.00	1.66			2.64					
$H/V_{Ave}$	2.36	2.06	1.77	1.83	2.62	2.28	1.92	2.31	2.71	5.65	3.15
$A^*$	2.08	1.95	2.67	1.34	2.79	1.52	1.25	2.30	2.16	2.40	2.70
$A$	1.69	1.60	1.37	1.21	1.37	1.79	1.71	1.63	1.50	1.66	1.57
AHSA	1.49	1.35	1.08	0.85	1.04	1.63	1.52	1.40	1.22	1.44	1.31

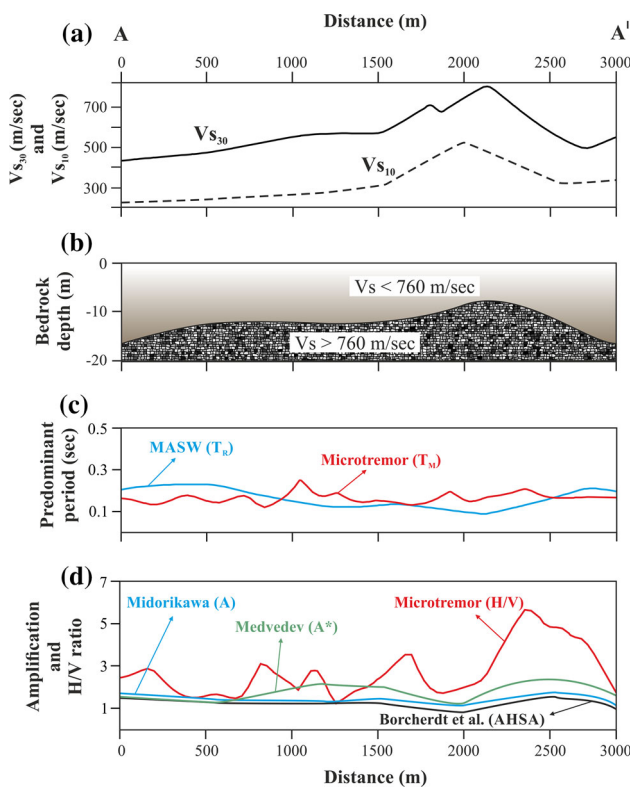


**Fig. 19** AA' cross section; **a**  $V_{S30}$  and  $V_{S10}$  changes, **b** the depth models obtained from  $V_S$  values, **c** comparison of predominant periods ( $T_M$  and  $T_R$ ), **d**  $H/V$  ratio and soil amplifications ( $A$ ,  $A^*$  and AHSA)

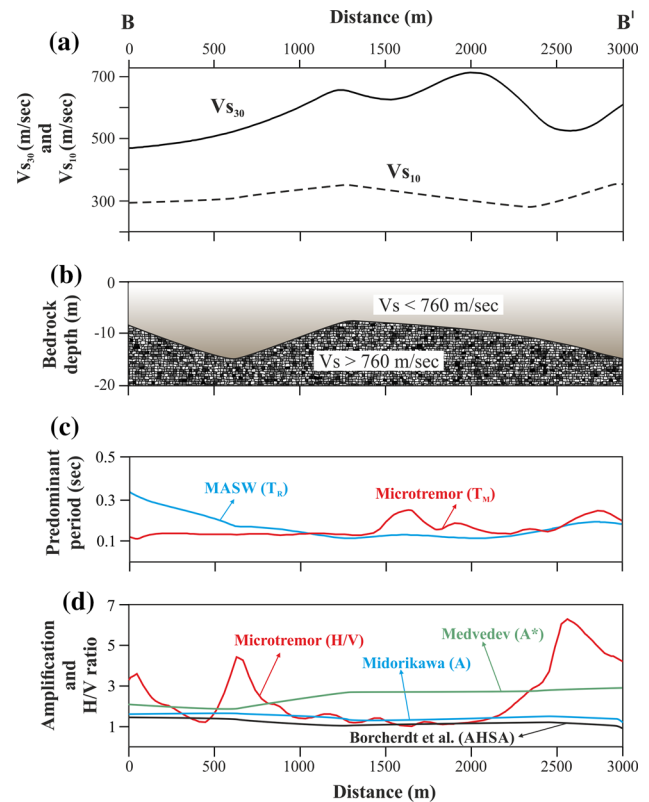


**Fig. 20** BB' cross section; **a**  $V_{S30}$  and  $V_{S10}$  changes, **b** the depth models obtained from  $V_S$  values, **c** comparison of predominant periods ( $T_M$  and  $T_R$ ), **d**  $H/V$  ratio and soil amplifications ( $A$ ,  $A^*$  and AHSA)

AHSA are in harmony, but the  $H/V$  spectral ratio deviates from them at many points.

**Acknowledgments** This study has been achieved under the scope of no: 11521 of the scientific research project (Karadeniz Technical University).

## References

- Adıgüzel Engineering (2012) Geologic drilling soil survey project for Arsin center Elementary school building, G43B04D3D sheet, block of buildings 215, sheet number 2 (no: 5094) Arsin-Trabzon
- Bard PY (2008) The  $H/V$  technique: capabilities and limitations based on the results of the SESAME project, Foreword. *Bull Earthq Eng* 6:1–2
- Bindi D, Parolai S, Spallarossa D, Cattaneo M (2000) Site effects by  $H/V$  ratio: comparison of two different procedures. *J Earthq Eng* 4:97–113
- Bonilla LF, Steidl JH, Lindley GT, Tumarkin AG, Archuleta RJ (1997) Site amplification in the San Fernando Valley, California: variability of site-effect estimation using the S-wave, coda, and  $H/V$  methods. *Bull Seismol Soc Am* 87:710–730
- Borcherdt RD, Wentworth CM, Glassmoyer G, Fumal T Mork P, Gibbs J (1991) On the observation and predictive GIS mapping of ground response in the San Francisco Bay region, California: fourth international conference on seismic zonation, Stanford, California, proc., III, pp 545–552
- Bour M, Fouissac D, Domonique P, Martin C (1989) On the use of microtremor recordings in seismic microzonation. *Soil Dyn Earthq Eng* 17(7–8):465–474
- Chatelain JL, Guillier B, Cara F et al (2008) Evaluation of the influence of experimental conditions on  $H/V$  results from ambient noise recordings. *Bull Earthq Eng* 6(1):33–74
- Chopra S, Kumar D, Rastogi BK, Choudhury P, Yadav RBS (2013) Estimation of site amplification functions in Gujarat region, India. *Nat Hazards* 65:1135–1155
- D'Amico V, Picozzi M, Baliva F, Albarello D (2008) Ambient noise measurements for preliminary site-effects characterization in the urban area of Florence, Italy. *Bull Seismol Soc Am* 98:1373–1388
- Eyüboğlu Y, Chung SL, Santosh M, Dudasi FO, Akaryali E (2011) Transition from shoshonitic to adakitic magmatism in the eastern Pontides, NE Turkey: implications for slab window melting. *Gondwana Res* 19:413–429
- Field EH, Jacob KH (1993) The theoretical response of sedimentary layers to ambient noise. *Geophys Res Lett* 24:2925–2928
- GEOPSY (1997) Geophysical signal database for noise array processing ([www.geopsy.org](http://www.geopsy.org))
- Guillier B, Atakan K, Chatelain JL et al (2008) Influence of instruments on  $H/V$  spectral ratios of ambient vibrations. *Bull Earthq Eng* 6(1):3–31
- Guven İH (1993) Geology map of East Pontides (1/25000) and complication. MTA, Ankara (**in Turkish**)
- Joyner WB, Fumal T (1984) Use of measured shear-wave velocity for predicting geological site effects on strong motion. In: *Proceedings of 8th world conference on earthquake engineering*, vol 2, pp 777–783
- Kanai K (1983) *Engineering Seismology* 251 University of Tokyo, Japonya
- Kanai K, Tanaka AT (1961) On microtremors VII. *Bull Earthq Res Inst* 39:97–114
- Kazmin VG, Sborshikov IM, Ricou LE, Zonenshain LP, Boulin J, Knipper AL (1986) Volcanic belts as markers of the Mesozoic–Cenozoic active margin of Eurasia. *Tectonophysics* 123:123–152
- Keçeli A (1996) The soil predominant period and soil allowable stress in engineering geophysics, conference notes (unpublished)
- Keskin S, Pedoja K, Bektaş O (2011) Coastal uplift along the eastern Black Sea coast: new marine terrace data from eastern Pontides (Turkey) and a review. *J Coast Res* 27(6A):63–73
- Konno K, Ohmachi T (1998) Ground-motion characteristics estimated from spectral ratio between horizontal and vertical components. *Bull Seismol Soc Am* 88(1):228–241
- Kurt Engineering (2008) Geological and geotechnical research project of Arsin-Trabzon fill sites (no: 2774) Trabzon
- Lachet C, Bard PY (1994) Numerical and theoretical investigation on the possibilities and limitations of the Nakamura's technique. *J Phys Earth* 42:377–397
- Lermo J, Chavez-Garcia FJ (1994) Site effect evaluation at Mexico City: dominant period and relative amplification from strong motion and microtremor records. *Soil Dyn Earthq Eng* 13:413–423
- Levenberg K (1944) A method for the solution of certain non-linear problems in least squares. *Q Appl Math* 2:164–168
- Leyton F, Ruiz S, Sepulveda SA, Contreras JP, Rebolledo S, Astroza M (2013) Microtremors' HVSR and its correlation with surface geology and damage observed after the 2010 Maule earthquake (Mw 8.8) at Talca and Curico central Chile. *Eng Geol* 161:26–33
- Liu HP, Boore DM, Joyner WB et al (2000) Comparison of phase velocities from array measurements of Rayleigh waves associated with microtremors and results calculated from borehole shear-wave velocity profiles. *Bull Seismol Soc Am* 90:666–678
- Louie JN (2001) Faster, better: shear-wave velocity to 100 meters depth from refraction microtremor arrays. *Bull Seismol Soc Am* 91(2):347–364
- Marquardt D (1963) An algorithm for least-squares estimation of nonlinear parameters. *SIAM J* 11:431–441
- Medvedev SS (1965) *Engineering seismology*, translated from Russian, Israel Program for Scientific Translations Jerusalem
- Midorikawa S (1987) Prediction of isoseismal map in the Kanto plain due to hypothetical earthquake. *J Struct Eng* 33b:43–48 (**in Japanese with English abstract**)
- Mucciarelli M (1998) Reliability and applicability of Nakamura's technique using microtremor: an experimental approach. *J Earthq Eng* 2:625–638
- Nakamura Y (1989) A method for dynamic characteristics estimation of sub-surface using microtremor on the ground surface. *Q Rep Railway Tech Res Inst* 30(1):25–33
- Nikishin AM, Korotaev MV, Ershov A, Brunet MF (2003) The Black Sea basin: tectonic history and Neogene–Quaternary rapid subsidence modelling. *Sedim Geol* 156:149–168
- Nogoshi M, Igarashi T (1971) On the amplitude characteristic of microtremor, part II. *J Seismol Soc Jpn* 24:26–40
- Okada H (2003) The microtremor survey method (geophysical monograph series no. 12). *Soc Explor Geophys Tulsa* 135
- Pando M, Cano L, Suárez LE, Ritta R, Montejó LA (2008) Comparison of site fundamental period estimates using weak-motion earthquakes and microtremors. In: *The 14th world conference on earthquake engineering*, 12–17 Oct 2008, Beijing, China
- Park CB, Miller RD, Xia J (1999) Multi-channel analysis of surface waves. *Geophysics* 64(3):800–808
- Park CB, Miller RD, Miura H (2002) Optimum field parameters of an MASW survey expanded abstract. *Soc Explor Geophys Jpn*, Tokyo
- Parolai S, Bormann P, Milkereit C (2001) Assessment of the natural frequency of the sedimentary cover in the Cologne area (Germany) using noise measurements. *J Earthq Eng* 5:541–564



- Parolai S, Orunbaev S, Bindi D, Strollo A et al (2010) Site effect assessment in Bishkek (Kyrgyzstan) using earthquake and noise recording data. *Bull Seismol Res Lett* 100:3068–3082
- Picozzi M, Strollo A, Parolai S et al (2009) Site characterization by seismic noise in Istanbul, Turkey. *Soil Dyn Earthq Eng* 29(3):469–482
- Rastogi BK, Singh AP, Sairam B, Jain SK, Kaneko F, Segawa S, Matsuo J (2011) The possibility of site effects: the Anjar case, following the past earthquakes in the Gujarat, India. *Seismol Res Lett* 82:59–68
- Rodriguez HS, Midorikawa S (2002) Applicability of the H/V spectral ratio of microtremors in assessing site effects on seismic motion. *Earthq Eng Struct Dyn* 31:261–279
- SeisImager/Pickwin (2014) [http://www.geometrics.com/geometric\\_sproducts/seismographs/download-seismograph-software/](http://www.geometrics.com/geometric_sproducts/seismographs/download-seismograph-software/)
- SESAME (2004) Guidelines for the implementation of the H/V spectral ratio technique on ambient vibrations: measurements, processing and interpretation SESAME European Research Project P12-Deliverable. D23.12 <ftp://ftp.geo.uib.no/pub/seismo/Software/Sesame/Userguidelines/Sesame-HV-UserGuidelines.doc>
- Singh AP, Annam N, Kumar S (2014) Assessment of predominant frequencies using ambient vibration in the Kachchh region of western India: implications for earthquake hazards. *Nat Hazards*. doi:10.1007/s11069-014-1135-2
- TPAO/BP Eastern Black Sea Project Study Group (1997) A promising area in the eastern Black Sea. The Leading Edge 1001
- Underground Research Centre (2012) Soil survey project of high security forensic psychiatric hospital building with 50 Beds Güzelyalı district block buildings 147 sheet number 3 (no: 3146) Arsin-Trabzon